CHAPTER- 3

Details of Catalysts Synthesis and Characterization

3.1. Introduction

In evaluating potential catalysts for NO_x reduction, catalytic activity, selectivity, and thermal stability are the most critical factors. An established norm is to conduct lab-scale testing of possible catalysts and analyse their material characteristics before conducting bench-scale or commercial-scale tests. The first step to developing new and improved catalytic formulations for large-scale applications is demonstrating the desired performance of the catalyst in lab-scale testing supported by their favourable physicochemical properties. Experimental conditions are always adjusted accordingly to measure the intrinsic activity of catalytic formulations effectively without masking the results by mass and energy transfer constraints. Thus, to give a fair idea about the experiments that have been done, this chapter provides an overview of the current state-of-the-art methods and methods for testing and characterization of catalysts.

3.2. Supports and catalyst synthesis

3.2.1. Ceria support synthesis

Three different ceria morphologies (nanorods, nanocubes, and nanopolyhedral) were synthesized using the hydrothermal method. In this process, an aqueous solution containing $Ce(NO_3)_3 \cdot 6H_2O$ was combined with a solution of the precipitant agent, NaOH, and mixed continuously at room temperature for uniform solution. The obtained mixtures were next placed into 100 ml Teflon-lined autoclaves to complete the hydrothermal process. The reaction temperature and time were then changed based on the desired morphologies of CeO_2, which is

given in **Table 3.1**. The resulting precipitates were cooled to room temperature after the hydrothermal process, and ethanol and deionized water were then used for washing to remove any potential ionic impurities. The subsequent precipitate was dried overnight at 65°C before being calcined for 4h at 500°C. The resultant samples were denoted by CeO_2-NR, CeO_2-NC, and CeO_2-NP for CeO_2-nanorod, CeO_2-nanocube, and CeO_2-nanopolyhedral, respectively, in the manuscript.

Table 3.1. Condition for different CeO_2 morphologies

Morphology	**Cerium *nitrate*** **(mole)**	**C_{NaOH}** **(mole)**	**Temperature** **(^oC)**	**Time** **(h)**
CeO_2-NR	5	7	100	12
CeO_2-NC	5	15	180	24
CeO_2-NP	4.5	8.5	180	24

3.2.2. Catalysts synthesis

3.2.2.1. MnO_x/CeO_2-NR catalyst

MnO_2, MnO, and Mn_2O_3 metal oxides were impregnated on the CeO_2-NR using the wet-impregnation method. The calculated amount (5wt.%) of commercial MnO_2, MnO, and Mn_2O_3 were mixed into the solution of CeO_2-NR, and mixtures were stirred till the metal oxide and support got homogeneously mixed. Then the homogenous solution was put in an air oven for drying at 100℃ overnight, followed by calcination at 500℃ for 4 h. These synthesized catalysts are denoted as MnO_2/CeO_2-NR, MnO/CeO_2-NR, and Mn_2O_3/CeO_2-NR.

3.2.2.2. Different phases of MnO_2 in the MnO_2/CeO_2-NR catalyst

The α-MnO_2 phase was synthesized by mixing 1.2 gm of $KMnO_4$ in 60 ml of deionized water with 0.5 gm of $MnSO_4.H_2O$ for 30 minutes at ambient temperature under magnetic stirring

until the homogenous solutions. Afterward, homogeneous solutions were put into a 100 ml Teflon-lined stainless-steel autoclave, sealed, and kept at 140°C for 12 h. The obtained precipitate was later washed several times with deionized water and ethanol and filtered to remove any undesirable ions. The precipitate was then dried in an oven at 105°C overnight. The β-MnO_2 phase was synthesized by taking 0.5 gm of $KMnO_4$ and 2.5 gm of $MnSO_4.H_2O$, while for the δ-MnO_2 phase, 2.8 gm of $KMnO_4$ and 0.5 gm of $MnSO_4.H_2O$ were taken and the other conditions were same as the α- MnO_2. The γ-MnO_2 phase was synthesized by mixing 3.7 gm of $(NH_4)_2S_2O_8$ with 2.7 gm of $MnSO_4$ for 30 minutes for a homogeneous mixture and transferred it into an autoclave at 90°C for 24 h. All the phases of MnO_2 were further calcined for 2 h at 300 °C.

The wet-impregnation method was used to impregnate the active metals on support. For these, specific amounts (5 wt.%, 8 wt.%, 11 wt.%, 13 wt.%, and 17 wt.%) of active metals and supports were added into de-ionized water and stirred till both were mixed homogenous. The obtained solution was put in an oven for drying at 105°C overnight, followed by calcination at 350°C for 4 h. The catalysts were denoted as α-MnO_2/CeO_2-NR, β-MnO_2/CeO_2-NR γ-MnO_2/CeO_2-NR, and δ-MnO_2/CeO_2-NR.

3.3. Characterization techniques

The structure of catalysts can provide insight into the interrelationship between catalyst preparation parameters and catalytic performance. It may also be necessary to characterize catalysts, i.e., to investigate relevant aspects of their structural features. The information generated by the characterization of the catalyst helps to optimize catalytic processes and synthesized the catalyst. It is important to understand the interrelationship between a catalyst's activity and selectivity and its various physical and chemical properties through its characterization. Several methods were used to characterize the support and catalysts by using Brunauer–Emmett–Teller (BET), X-ray diffraction, X-ray photoelectron spectroscopy,

transmission electron microscopy, scanning electron microscopy, energy dispersive X-ray analysis, temperature-programmed reduction, and Raman spectroscopy and are shown in **Table 3.2**.

Table 3.2. Different characterizations techniques used for anaylzed the samples

S. No.	Instrument	Application
1.	Brunauer–Emmett–Teller	Anaylzed the surface area, pore volume, and pore diameter
2.	X-Ray Diffraction	Crystal structure- phase identification and crystallite size
3.	X-ray Photoelectron Spectroscopy	Element composition and oxidation state of elements
4.	Transmission Electron Microscope	Imaging and particle size
5.	Scanning Electron Microscopy	Morphology analysis
6.	Energy Dispersive X-ray Analysis	Surface elemental analysis
7.	Temperature-Programmed Reduction	Surface chemistry of metals and metal oxides
8.	Raman Spectroscopy	Chemical composition of materials

3.3.1. Brunauer Emmett and Teller (BET)

Determination of surface area and pore distribution of catalysts is important to understand the extent of dispersion possible for the active metals. Higher surface area of support results in higher dispersion of the active metals. Hence supports of higher surface area are desirable. Pores are usually formed during drying or calcination of hydroxides precipitates or gel. The size and number of pores determines the internal surface area. Pore size also determines the accessibility of reactants to the active sites and the ability of diffusion of products back to the

bulk fluid. Hence pore structure and surface area must be optimized to provide maximum utilization of active sites for a given feed stock.

Gas adsorbs on internal and external surfaces of a porous material in equilibrium at temperature (T) and relative vapor pressure p/p_0. The relation between relative vapor pressure and amount of gas adsorbed at constant temperature is known as adsorption isotherm. An adsorption isotherm of porous materials is determined by adsorption and condensation of liquid N_2 at 77°K.

The BET equation is used to calculate the surface area of porous materials. The principle of the BET model is that a gas adsorbs on the surface in a monolayer at a low relative pressure (multilayers arise at high pressure). The BET model calculates the number of moles of adsorbate (n) adsorbed on 1 gm of the sample with the applied gas pressure (P) by using equation 3.1:

$$\frac{P/P_o}{n(1-\frac{P}{P_o})} = \frac{1}{n_m c} + \frac{c-1}{n_m c}\left(\frac{P}{P_o}\right) \qquad (3.1)$$

where;

n_m = the estimated number of moles that are monolayer-adsorbed on 1 gm of adsorbent,

P = the gas pressure,

P_o = saturated vapour pressure of gas

c = constant

In this study, specific surface area ($m^2.g^{-1}$), pore volume ($cm^3.g^{-1}$) and average pore diameter (Å) of support and catalysts were anaylzed through ASAP 2020 (micromeritics, USA) Brunauer-Emmett-Teller (BET) analyzer, using the N_2 adsorption at temperature (-196°C). The samples were degassed at 200°C for 6 h before adsorption measurements. [1-3]

3.3.2. X-Ray Diffraction (XRD)

X-ray diffraction (XRD) is a highly utilized and reliable method for precisely determining the atomic positions in various types of matter, including fluids, powders, and perfect crystals. It is a non-destructive technique widely employed for the characterization of crystalline materials. XRD offers valuable information about the structure of materials, including identifying different crystal phases present, the preferred orientation of crystals, and various structural parameters. Some of the key structural parameters obtained from XRD analysis include lattice parameters, which define the size and shape of the crystal unit cell, as well as parameters related to crystallite size, crystallite shape, strain, and crystal defects. The diffraction patterns are produced when X-rays interact with the crystal lattice. The diffraction pattern provides information about the spacing between crystal planes, known as d-spacing, and the angles at which the X-rays are diffracted. XRD is particularly valuable for identifying the crystal structure of unknown materials, quantifying the phase composition in mixtures, and monitoring phase changes in materials due to temperature or other external factors.

This research anaylzed the synthesized samples through the Rigaku Miniflex (Rigaku Corporation, Japan) X-ray diffractometer with Ni-filtered Cu Ka radiation (λ = 1.5406 Å) working at 40 kV and 15 mA. Diffraction ranges were recorded in the scan range of 10-80° and at a scanning rate of 6°/minute. The phase identification was justified by matching the XRD with JCPDS reference data. The crystallite size of the synthesized samples was determined using the Scherrer equation:

$$d = \frac{0.89\lambda}{\beta cos\theta} \qquad (3.2)$$

where d, λ, θ, and β are the parameters for the crystallite size, X-ray wavelength (1.518Å), Bragg diffraction angle and full width at half maximum (FWHM) of the diffraction peak, respectively. [4-6]

3.3.3. X-Ray Photoelectron Spectroscopy (XPS)

X-ray Photoelectron Spectroscopy is a powerful spectroscopic technique that provides quantitative analysis of the elemental composition of a material's surface. It offers valuable information about the empirical formula of pure materials; chemical and electronic states of the elements present within the material and the uniformity of elemental composition across the top surface. By bombarding the material's surface with X-rays, XPS causes the emission of photoelectrons. The energies of these emitted electrons are then measured, allowing for the identification and quantification of the elements present. This technique also provides insights into the elements' chemical bonding and oxidation states, giving information about the chemical environment and interactions within the material. Furthermore, XPS is sensitive to surface contamination, allowing for the detection and characterization of foreign elements or impurities that may be present on the surface. It also provides information about the spatial distribution of elements, giving an understanding of the uniformity or variations in elemental composition across the top surface of the material. [7-9]

This study collected XPS data through the Amicus spectrometer equipped with Mg Kα X-ray radiation to anaylzed XPS. It operated at 15 kV and 12 mA for the typical analysis, and pressure was less than 105 Pa, which was maintained to maintain a vacuum environment. To calibrate the binding energy scale, 284.7 eV was selected as the primary C 1s line of adventitious impurities.

3.3.4. Scanning Transmission Electron Microscopy (STEM)

STEM allows researchers to obtain high-resolution images of nanoscale samples and provide information about the material's structure. TEM instruments transmit electrons through a material at high energies (usually 100 kV to 300 kV) and an image is obtained by collecting electrons transmitted by the transmission electron microscope. The TEM instrument used throughout the work presented here was the JEOL JEM-2100 electron microscope operated at

200 kV. The samples were firstly dispersed into alcohol using ultrasonography and then put on the copper grid. [10-11]

3.3.5. Scanning Electron Microscopy- Energy-Dispersive X-ray analysis (SEM-EDX)

This study employed scanning electron microscopy (SEM) for morphological characterization. SEM enables the estimation of various properties, such as the average aggregate size, crystallinity degree of oxides, and microstructures of powders. One of the advantages of SEM analysis is its non-destructive nature, as the x-rays generated by electron interactions do not cause any loss of sample volume. This allows repeated analysis of the same materials. In SEM, topographical images are generated by back-scattered primary or low-energy secondary electrons. The resolution of SEM typically ranges from 2 to 5 nm, although lower resolutions are often sufficient for routine studies. SEM takes advantage of image interpretation and the exceptional depth of field to provide a comprehensive view of the specimen. This allows for examining the distribution and sizes of mesopores, which is particularly valuable for non-crystalline catalysts. Overall, SEM serves as a helpful tool in characterizing morphological features, providing detailed insights into the structures and properties of the examined materials. This study used scanning electron microscopy (SEM) equipped with dispersive energy X-ray (EDX) analysis (EVO-18-20-45). The samples were coated with a thin layer of gold before scanning. [12-14]

3.3.6. Temperature Programmed Reduction (TPR)

Temperature-programmed reduction (TPR) is widely used in catalysis characterization and screening. It plays a crucial role in understanding the surface chemistry of metals and metal oxides by subjecting them to varying thermal conditions. [15-16]

The catalysts in this research were tested on the Micropolitics instrument Chemisorb 2720 (USA) to anaylzed the reducibility of the catalysts. The 0.1 gm of synthesized catalysts were

used for H_2-TPR analyses from room temperature to 700°C with a heating rate of 10°C - min^{-1} in an H_2 (5 vol.%) stream diluted in Ar.

3.3.7. Raman Spectroscopy

In Raman spectroscopy, molecules, and crystals are studied for their internal structural details. The mechanism relies on the dispersion of electromagnetic radiation by molecules. Molecular transitions such as rotation, vibration, and other low-frequency transitions can be observed by the Raman shift. It is used to look at molecular structures qualitatively. Because of the low sensitivity of Raman scattering, it is often not used for quantitative studies. Along with IR spectroscopy, Raman spectroscopy is also helpful for fingerprinting. Molecule scattering can be elastic or inelastic. Scattering is described into two types. One is elastic scattering, also known as Rayleigh scattering, in which the scattered light has the same frequency as the radiation from the source. The other is inelastic scattering, also known as Raman scattering, in which the scattered light has a different frequency from the radiation source. A Renishaw Laser-type instrument operating at a wavelength of 532 nm was used in the current study to measure the Raman spectra. The Raman shift was measured between 100 and 2000 cm^{-1}. [17-18]

3.4. Catalytic Evaluation

The NH_3-SCR reaction was carried out by charging 0.4 g catalyst (40-60 mesh) in an Inconel tubular reactor (ID 12 mm x long 500 mm) at atmospheric pressure (**Fig. 3.1**). A feed mixture of 1000 ppm NO, 1000 ppm NH_3, 6% O_2 and rest argon as balance at total flow rate of 100 mL min^{-1}, corresponding to a space velocity of 13,000 h^{-1} was fed to the reactor. A thermocouple was inserted inside the reactor and connected through a programmable temperature controller to monitor the reaction conditions. All the gas flow rates were controlled through Bronkhorst mass flow controller. Prior to the reaction, the catalyst was activated in a flow of 5% H_2 gas at 400°C for 3 h. The inlet and outlet reactor gas concentration of NO were anaylzed by a

chemiluminescence (UNIPHOS ENVIROTRONIC Pvt Ltd, India). A Centurion Scientific, 5800 model Gas Chromatography (GC) with TCD was used for the identification of N_2, O_2 and N_2O.

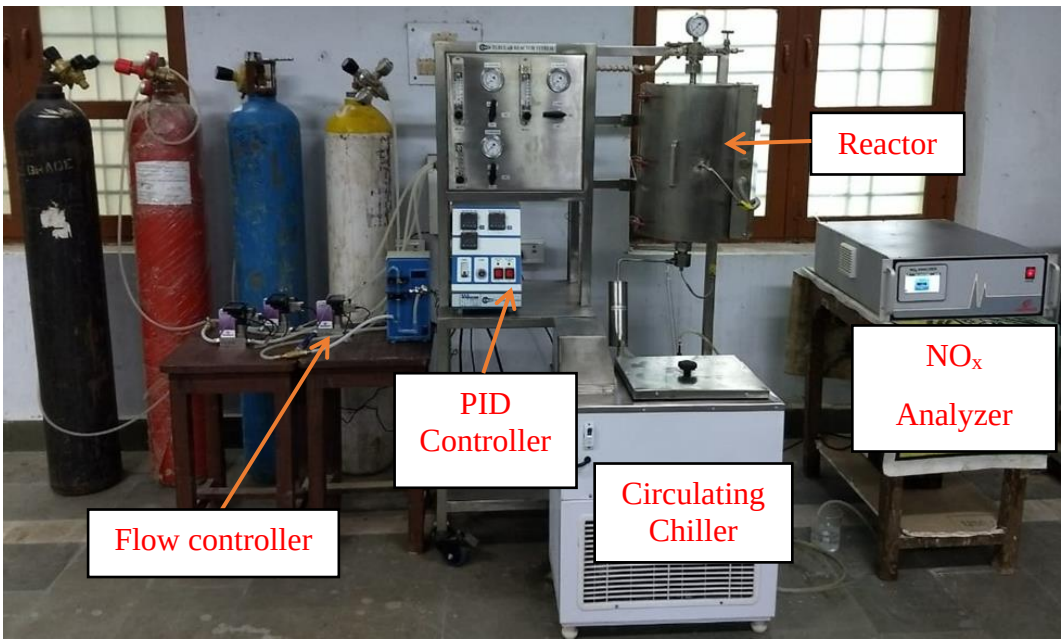

Fig. 3.1. General view of the experiment assembly in the lab

The catalyst performance was calculated using the turnover frequency (TOF), NO conversion, and N_2 selectivity. The NO_x conversion is a proportion of the NO_x reactant amount to the amount injected into the reactor.

$$NO_x \text{ Conversion} = \frac{(NO)_{inlet} - (NO)_{outlet}}{(NO)_{inlet}} \times 100\ (\%) \qquad (3.1)$$

$$N_2 \text{ Selectivity} = \frac{(N_2)}{(NO)_{inlet} - (NO)_{outlet}} \times 100\ (\%) \qquad (3.2)$$

where, $(NO)_{inlet}$ and $(NO)_{outlet}$ represents the molar flow rate of NO at the inlet and out in the reactor respectively.

The turnover frequency (TOF) is defined as the number of moles of product per mole of catalyst per unit time or the turnover number per unit time. This quantity has units of sec^{-1} and represents, the number of molecules reacting per (chemisorption) site per second.

$$\text{TOF } [s^{-1}] = \frac{F_{NO}\,[L\,min^{-1}] \times NO_{Conversion}\,[\%]}{m[g] \times H_{2_{Consumption}}\,[mol\,g^{-1}] \times 2 \times 22.4\,[L\,mol^{-1}] \times 60\,[s\,min^{-1}]} \qquad (3.3)$$

Turn over frequency is one of the most important parameters to represent the performance of catalyst. It relates the NO conversion with catalytic active sites of catalysts.

Rate of reaction is important parameter, which is used in calculation activation energy of the samples.

$$\text{Reaction rate [mol. } g^{-1}\text{. cats}^{-1}] = \frac{X_{NO}[\%] X\, F_{NO}[L min^{-1}]}{60\ X\ [s min^{-1}]\ X\ 22.4\ [L min^{-1}]\ X\ m_{cat}[g]} \qquad (3.4)$$

where, $(m)_{cat}$= weight of catalyst [gm], X_{NO}= NO conversion [%], and F_{NO} = NO flow rate [L. min^{-1}].

References

1. Bardestani, R., Patience, G.S. and Kaliaguine, S., 2019. Experimental methods in chemical engineering: specific surface area and pore size distribution measurements—BET, BJH, and DFT. The Canadian Journal of Chemical Engineering, *97*(11), pp.2781-2791.
2. Brizes, M., Sepe, M., Satjaritanun, P., Shimpalee, S. and Weidner, J.W., 2019, September. Characterization of Gas Diffusion Layers through Computational Fluid Dynamics Modelling and BET Theory. In Electrochemical Society Meeting Abstracts *236* (No. 54, pp. 2357-2357). The Electrochemical Society, Inc.
3. Osterrieth, J.W., Rampersad, J., Madden, D., Rampal, N., Skoric, L., Connolly, B., Allendorf, M.D., Stavila, V., Snider, J.L., Ameloot, R. and Marreiros, J., 2022. How reproducible are surface areas calculated from the BET equation? *Advanced Materials*, *34*(27), p.2201502.
4. Tsirelson, V.G. and Ozerov, R.P., 2020. Electron density and bonding in crystals: Principles, theory and X-ray diffraction experiments in solid state physics and chemistry. CRC Press.
5. Abe, M., Suzuki, R., Kojima, K. and Tachibana, M., 2020. Evaluation of crystal quality of thin protein crystals based on the dynamical theory of X-ray diffraction. *IUCrJ*, *7*(4), pp.761-766.
6. Zhang, F., Örnek, C., Liu, M., Müller, T., Lienert, U., Ratia-Hanby, V., Carpén, L., Isotahdon, E. and Pan, J., 2021. Corrosion-induced microstructure degradation of copper in sulphide-containing simulated anoxic groundwater studied by synchrotron high-energy X-ray diffraction and ab-initio density functional theory calculation. *Corrosion Science*, *184*, p.109390.

7. Osterman, C. and Fundin, A., 2020. A systems theory for lean describing natural connections in an XPS. *The TQM Journal*, *32*(6), pp.1373-1393.
8. Krishna, D.N.G. and Philip, J., 2022. Review on surface-characterization applications of X-ray photoelectron spectroscopy (XPS): Recent developments and challenges. *Applied Surface Science Advances*, *12*, p.100332.
9. Lefebvre, J., Galli, F., Bianchi, C.L., Patience, G.S. and Boffito, D.C., 2019. Experimental methods in chemical engineering: X-ray photoelectron spectroscopy-XPS. *The Canadian Journal of Chemical Engineering*, *97*(10), pp.2588-2593.
10. López, N., Morgan, D.L., Hutchings, Q.R. and Davis, K., 2022. Revisiting critical STEM interventions: A literature review of STEM organizational learning. *International Journal of STEM Education*, *9*(1), p.39.
11. Wang, M., Hu, Y., Pu, J., Zi, Y. and Huang, W., 2023. Emerging Xene-based Single-Atom Catalysts: Theory, Synthesis and Catalytic Applications. *Advanced Materials*, p.2303492.
12. Badri, A., Slimi, S., Guergueb, M., Kahri, H. and Mateos, X., 2021. Green synthesis of copper oxide nanoparticles using Prickly Pear peel fruit extract: Characterization and catalytic activity. *Inorganic Chemistry Communications*, *134*, p.109027.
13. Liu, X., Pajares, A., Matienzo, D.D.C., de la Piscina, P.R. and Homs, N., 2020. Preparation and characterization of bulk MoXC catalysts and their use in the reverse water-gas shift reaction. *Catalysis Today*, *356*, pp.384-389.
14. Ma, X., Zhou, F., Yue, H., Hua, J. and Ma, P., 2019. A nano-linear zinc-substituted phosphomolybdate with reactive oxygen species catalytic ability and antibacterial activity. *Journal of Molecular Structure*, *1198*, p.126865.
15. Dai, W., Li, Z., Li, C., Zhang, C., Wang, F., Liu, P. and Qiao, H., 2023. Revealing the effects of preparation methods over Ce-MnO_x catalysts for soot combustion:

physicochemical properties and catalytic performance. *Journal of Industrial and Engineering Chemistry*.

16. Wang, C., Yan, W., Wang, Z., Chen, Z., Wang, J., Wang, J., Wang, J., Shen, M. and Kang, X., 2020. The role of alkali metal ions on hydrothermal stability of Cu/SSZ-13 NH3-SCR catalysts. *Catalysis Today*, *355*, pp.482-492.
17. Zhang, H., Duan, S., Radjenovic, P.M., Tian, Z.Q. and Li, J.F., 2020. Core–shell nanostructure-enhanced Raman spectroscopy for surface catalysis. *Accounts of Chemical Research*, *53*(4), pp.729-739.
18. Hess, C., 2021. New advances in using Raman spectroscopy for the characterization of catalysts and catalytic reactions. *Chemical Society Reviews*, *50*(5), pp.3519-3564.